ARTICLES

Quenching Mechanism of Excited Coronene by a Nitroxide Radical Studied by Probing Dynamic Electron Polarization

Masaaki Mitsui,[†] Yasuhiro Kobori,[‡] Akio Kawai,* and Kinichi Obi[§]

Department of Chemistry, Graduate School of Science and Engineering, Tokyo Institute of Technology, 2-12-1 Ohokayama, Meguro-ku, Tokyo 152-8551, Japan

Received: September 9, 2003; In Final Form: November 18, 2003

By use of the time-resolved electron spin resonance (TR-ESR) method, quenching mechanisms of S_1 and T_1 coronene by the 2,2,6,6-tetramethylpiperidine-1-oxyl (TEMPO) radical were investigated by probing absorptive (abs) and emissive (em) chemically induced dynamic electron polarizations (CIDEP), which are generated by interactions of S_1 and T_1 coronene with TEMPO radicals, respectively. Absolute magnitudes of abs and em CIDEPs created on TEMPO radicals in the coronene−TEMPO system in benzene were determined as 1.8 and 2.2, respectively, in the units of Boltzmann polarization by utilizing Bloch and kinetic equations. This result is evaluated by a theoretical model that describes the magnitude of CIDEP created in the radical−triplet (RT) system, and it is clarified that exchange interaction of the T_1 coronene−TEMPO pair is much larger than the Zeeman energy and the em CIDEP is dominantly generated in the level-crossing regions. This means that quenching of T_1 coronene by TEMPO in benzene occurs through an electron-exchange interaction in an RT encounter complex. A ratio of em to abs CIDEP magnitudes was determined to be 1.2. The difference between the magnitudes of abs and em CIDEPs implies that the mean reaction distance of S_1 quenching is about 1−2 Å longer than that of T_1 quenching. This result suggests that an S_1−T_1 enhanced intersystem crossing occurs through both charge transfer and exchange mechanisms while T_1 quenching occurs only through exchange mechanism.

1. Introduction

The excited-state quenching of aromatic molecules by intermediate radicals occurs in numerous early photochemical and photobiological stages. The phenomena have been known for a long time and extensively investigated by optical measurements.[1−10] In these studies, chemically stable nitroxide radicals such as 2,2,6,6-tetramethylpiperidine-1-oxyl (TEMPO) have been used to understand the excited-state quenching by doublet species. More recently, quenching of excited states by radicals covalently linked to the excited molecule attracts much attention because of the growing interest of high-spin excited states of organic molecules such as quartet[11] and quintet states.[11c] Fluorescence probe molecules for free radicals also utilize the idea of excited-state quenching by free radicals.[12] These probe molecules include fluorescent and free-radical moieties, and intramolecular fluorescence quenching depresses fluorescence intensity. Once the radical moiety is destroyed by the reaction with a target free radical, fluorescence intensity increases to be detected by observer.

T_1 quenching by radicals in solution is in no case diffusion controlled. However, the quenching of the S_1 state is fast and in many cases diffusion controlled,[5−10] which seems to have no parallel relation with T_1 quenching.[1−4] So far, several mechanisms have been proposed to explain the excited-state quenching.[5−10] The mechanism of T_1 quenching is interpreted mostly by T_1−D_1 energy transfer or enhanced intersystem crossing (EISC). On the other hand, S_1 quenching by radicals may occur via the following different mechanisms.[5−10]

(A) Electron exchange in an encounter complex

$$^1M^* + {}^2R \rightarrow {}^2(^1M^* \cdots {}^2R) \rightarrow {}^3M^* + {}^2R \quad (1)$$

$$\rightarrow {}^1M + {}^2R \quad (2)$$

where the excited molecule ($^1M^*$) is converted to the triplet state ($^3M^*$) or the ground state (^1M) during the encounter with free radical (^2R).

(B) S_1−D_1 energy transfer

$$^1M^* + {}^2R \rightarrow {}^2(^1M^* \cdots {}^2R) \rightarrow {}^1M + {}^2R^* \quad (3)$$

(C) Charge transfer (CT) collision complex

$$^1M^* + {}^2R \rightarrow {}^2(^2M^{\pm} \cdots {}^1R^{\mp}) \rightarrow {}^3M^* + {}^2R \quad (4)$$

$$\rightarrow {}^1M + {}^2R \quad (5)$$

* Corresponding author. E-mail: akawai@chem.titech.ac.jp. Tel: +81-3-5734-2231. Fax: +81-3-5734-2655.

[†] Present address: Department of Chemistry, Keio University, 3-14-1 Hiyoshi, Kohoku-ku, Yokohama, Kanagawa 223-8522, Japan.

[‡] Present address: Department of Chemistry, University of Chicago, 5735 South Ellis Avenue, Chicago, IL 60637-1403.

[§] Present address: Department of Chemical and Biological Sciences, Japan Women's University, 2-8-1 Mejirodai, Bunkyo-ku, Tokyo 112-8681, Japan.

10.1021/jp036685h CCC: $27.50
Published on Web 01/03/2004

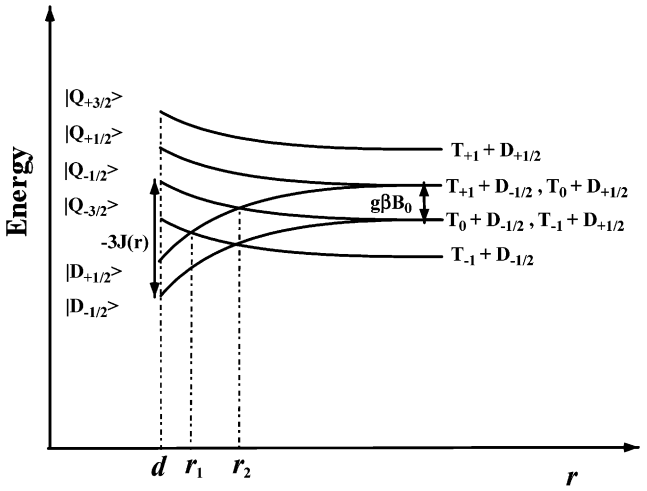

Figure 1. Schematic energy diagram of the spin states of the triplet−doublet encounter complex under external magnetic field, B_0. The exchange interaction, $J(r)$, of the RT pair is assumed to be negative.

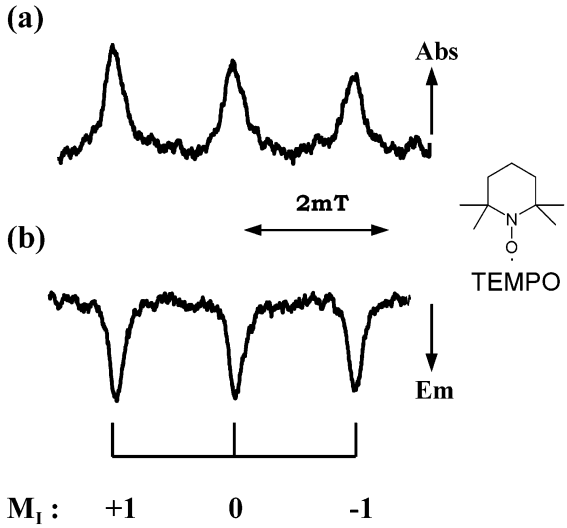

Figure 2. TR-ESR spectra of TEMPO in the Cor−TEMPO (0.16−1.2 mM) system in benzene obtained by a 308-nm excitation with gate times of (a) 0.5−1.0 μs and (b) 1.3−1.8 μs. M_I nuclear spin states of nitrogen atom are described in the figure.

Reactions 1−5 are spin allowed, and reactions 1 and 4 are S_1-T_1 EISC, while reactions 2, 3, and 5 enhance the internal conversion (S_1-S_0 EIC). Previous studies[5−10] have shown the fluorescence quenching by nitroxide radicals occurs mostly through S_1-T_1 EISC due to exchange or CT mechanisms to yield the T_1 state. It is noteworthy that both complexes of the encounter and CT have very short lifetimes, and it is difficult to distinguish reaction 1 from 4 in the S_1-T_1 EISC process.

Recent time-resolved electron spin resonance (TR-ESR) experiments show that chemically induced dynamic electron polarization (CIDEP) is created through interactions between excited molecules and free radicals.[13−20] This phenomenon is explained by magnetic interactions acting on the potential surfaces of spin states of radical−triplet (RT) pairs (Figure 1) and is interpreted in terms of the radical−triplet pair mechanism (RTPM). According to the RTPM, two patterns of CIDEP are observed on free radicals; one is a net emission (em) CIDEP observed in the T_1−radical system,[13,15−19,21] and the other is a net absorption (abs) CIDEP in the S_1−radical system.[15,16,19,20] In the T_1−radical system, randomly encountered pairs become quartet (Q) and doublet (D) spin states and the latter convert to the radical and ground-state singlet molecule pairs through T_1 quenching. As a result, a population of Q spin states ($|Q \pm m|$), where m is a magnetic quantum number, becomes higher than that of D spin states ($|D \pm m|$). During the encounter process, the Q and the D spin states mix with each other by zero-field splitting (zfs) interaction and a net em CIDEP is created. This mechanism is called a Q precursor RTPM (QP-RTPM).[16] In the S_1−radical system, S_1-T_1 EISC[14,16] selectively yields D spin states of RT pairs during S_1−radical random encounters. As a result, one observes a net abs CIDEP, which is in the opposite sign to that in the T_1−radical system. This is called a D precursor RTPM (DP-RTPM).[14] As one can observe, CIDEPs with various patterns and magnitudes, which are fingerprints of the intermolecular spin dynamics, quantitative information about the reaction dynamics of excited molecule-free radical systems can be obtained by comparing the data[17,19,21] with theoretical calculations.[21−23]

In this study, we examined CIDEP created in the quenching of the excited coronene(Cor)−TEMPO system to learn the EISC process. Cor has a relatively long fluorescence lifetime, and thus, it is easy to study both S_1 and T_1 quenching processes by using the Cor−TEMPO system as a model system. An absolute magnitude of net DP-RTPM polarization and a ratio of magnitudes of net DP-RTPM and QP-RTPM polarization in the Cor−TEMPO system were estimated from analyses of CIDEP time profile. A theoretical evaluation for the CIDEP magnitude is also presented. Possible mechanisms contributing to the S_1-T_1 EISC in S_1 quenching by TEMPO are discussed on the basis of experimental and theoretical results.

2. Experimental Section

TR-ESR Measurements. Transient ESR signals generated by XeCl excimer laser (Lambda Physik LPX 100, 308 nm) irradiation were detected by a diode of a conventional X-band ESR spectrometer (Varian E-112) without field modulation and were transferred to a boxcar integrator (Stanford SR-250) for TR-ESR spectrum measurements or a transient memory (Tektronix TDS 350) for CIDEP time profiles. A wide-band amplifier (LH0032 10 MHz) was inserted between the detection system and the signal analyzer for the transient ESR signals. Laser power was properly attenuated by a series of filters. Sample solutions were flowed through a flat cell (0.5 mm interior space) in the ESR cavity.

TR Thermal Lensing, Transient Absorption, and Fluorescence Measurements. The exciting light source was the XeCl excimer laser. Laser power was attenuated to the range where triplet−triplet annihilation was suppressed. The TR-thermal lensing (TL)[24] and transient absorption[25] apparatus were described elsewhere. The fluorescence lifetime was measured by the apparatus used in the transient absorption measurements without a monitoring light.

Samples. Cor was recrystallized from GR-grade benzene. *trans*-Stilbene and benzophenone (BP) were recrystallized from GR-grade *n*-hexane. GR-grade benzene and ethanol were used as solvents without further purification. TEMPO radical (Aldrich) was used as received. All the other chemicals were from Tokyo Kasei. Optical densities of sample solution were determined by the UV−vis spectrometer (Shimadzu UV2200). All sample solutions were thoroughly degassed by Ar gas, and measurements were carried out at room temperature.

3. Results and Discussion

3.1. CIDEP in Excited Cor Quenching. First, we review CIDEP created in the excited Cor−TEMPO system. Figure 2

shows TR-ESR spectra obtained by a 308-nm excitation of the Cor−TEMPO system in benzene at (a) 0.5−1.0 μs and (b) 1.3−1.8 μs. The triplet hyperfine structure indicates line splitting by a nitrogen atom, which suggests that these spectra are due to spin-polarized TEMPO. According to the DP-RTPM,[14,16] the abs-type CIDEP signal is generated in the S_1-T_1 EISC process caused by TEMPO radicals at an early time stage (Figure 2a). This CIDEP changes to em-type later (Figure 2b), which is generated in T_1 Cor quenching according to the QP-RTPM.[14,16] Similar CIDEP phase changes have been observed in the systems of fluoranthene−, pyrene−, naphtharene−,[14,16] and diphenylanthracene−TEMPO.

For quantitative discussion about magnitudes of net abs and em CIDEPs, we consider the reaction scheme as follows

$$\text{Cor} + h\nu\ (308\ \text{nm}) \rightarrow {}^1\text{Cor}^* \tag{6}$$

$${}^1\text{Cor}^* \xrightarrow{k_{ic}} \text{Cor} \tag{7}$$

$$\xrightarrow{k_f^0} \text{Cor} + h\nu_f\ (\text{fluorescence}) \tag{8}$$

$$\xrightarrow{k_{isc}} {}^3\text{Cor}^* \tag{9}$$

$${}^1\text{Cor}^* + \text{TEMPO} \rightarrow$$

$${}^2({}^1\text{Cor}^* \cdots \text{TEMPO}) \xrightarrow{k_{EISC}} {}^3\text{Cor}^* + {}^*\text{TEMPO} \tag{10}$$

$$\xrightarrow{k_{EIC}} \text{Cor} + \text{TEMPO} \tag{11}$$

$${}^3\text{Cor}^* \xrightarrow{k_T} \text{Cor} \tag{12}$$

$${}^3\text{Cor}^* + \text{TEMPO} \xrightarrow{k_q^T} \text{Cor} + {}^{**}\text{TEMPO} \tag{13}$$

^{1}Cor* and ^{3}Cor* represent S_1 and T_1 coronene, respectively. *TEMPO and **TEMPO represent radicals that have quenched ^{1}Cor* and ^{3}Cor* and are spin polarized by the DP-RTPM and the QP-RTPM, respectively. The k_{ic}, k_f^0, and k_{isc} are the rate constants for internal conversion, fluorescence, and S_1-T_1 ISC, respectively. k_{EISC} and k_{EIC} are the rate constants of S_1-T_1 EISC and S_1-S_0 EIC, respectively. It is noted that reaction 10 is the process that contributes to the net abs CIDEP generation. The k_T and k_q^T are the rate constants of unimolecular deactivation of ^{3}Cor* without TEMPO and quenching of ^{3}Cor* by TEMPO, respectively. The rate constants of fluorescence decay (k_f) and total S_1 quenching (k_q^S) are given by $k_f = k_{ic} + k_f^0 + k_{isc}$ and $k_q^S = k_{EISC} + k_{EIC}$, respectively. These kinetic parameters were determined as following.

3.2. Determination of Kinetic Parameters. The k_f, k_q^S, k_T, and k_q^T values were determined by time-resolved fluorescence and triplet−triplet absorption measurements. The fluorescence decays shown in the inset of Figure 3a were measured by monitoring 453-nm fluorescence in benzene. The fluorescence lifetime of 244 ns, i.e., $k_f = 4.1 \times 10^6\ s^{-1}$, was obtained by a single exponential-fitting analysis of the decay in the absence of TEMPO. The Stern−Volmer plots of the decay rates against TEMPO concentration shown in Figure 3a are on the straight line, and the slope of the fitted line gave k_q^S of $(4.5 \pm 0.3) \times 10^9\ M^{-1}\ s^{-1}$ ($M = mol/dm^3$). Figure 3b shows Stern−Volmer plots of ^{3}Cor* decay rates against TEMPO concentration. The time profiles of ^{3}Cor* were monitored at 490 nm as shown in the inset. The triplet decay rate constant in the absence of TEMPO was determined as $k_T = 5.45 \times 10^4\ s^{-1}$, and the slope of the fitted line gave k_q^T of $(8.5 \pm 0.4) \times 10^8\ M^{-1}\ s^{-1}$.

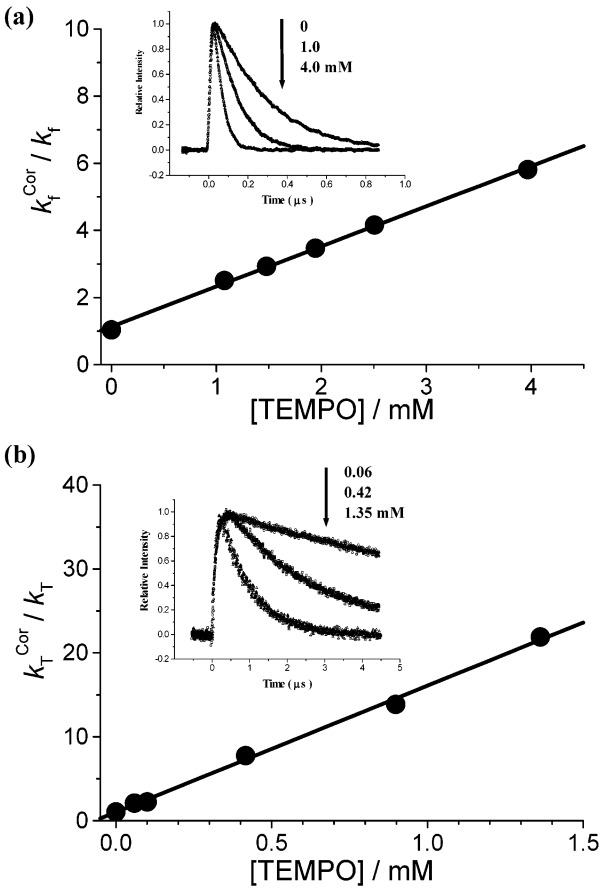

Figure 3. (a) Plots of Cor fluorescence decay rate constants, k_f^{Cor} divided by k_f against [TEMPO]. Inset: Fluorescence decays of Cor in benzene monitored at 453 nm with TEMPO concentrations of 0, 1.0, and 4.0 mM. (b) Plots of ^{3}Cor* decay rates, k_T^{Cor} divided by k_T against [TEMPO]. Inset: Decay curves of the transient absorption of ^{3}Cor* in benzene monitored at 490 nm with TEMPO concentrations of 0.06, 0.42, and 1.35 mM.

To determine k_{EISC}, we measured the quantum yield of ^{3}Cor* (Φ_T) against various TEMPO concentration by TR-TL method. Figure 4a shows a time profile of a TL signal of Cor with 0.2 mM of TEMPO in benzene. After the laser excitation, the TR-TL signal rises promptly due to a heat released by fast nonradiative processes and again rises slowly by slow nonradiative processes. The former and the latter signal intensities are defined as U_F and U_S. We measured similar TR-TL signals under various TEMPO concentrations (0−1.4 mM). Under the present experimental condition, U_S and total TR-TL signal intensity (U_T) linearly depended on laser power. This means the heat coming from the higher excited state prepared by the extra absorption process can be neglected. The heat conversion efficiency, γ, represents a ratio of the total heat released from the excited molecule to the excitation photon energy and is defined by the following equation

$$\gamma = \frac{E_{ex} - \Phi_{react} E_p}{E_{ex}} \tag{14}$$

where E_{ex}, Φ_{react}, and E_p are the photon energy of the excitation laser, the quantum yield of a certain photoreaction, and the energy stored by photoproducts, respectively. The γ value was determined by TR-TL measurements of the total heat released from the excited molecules. For calibration of the TL signal, BP was used as a calorimetric standard whose γ value is almost unity in benzene.[24] Figure 4b shows U_T against the photon

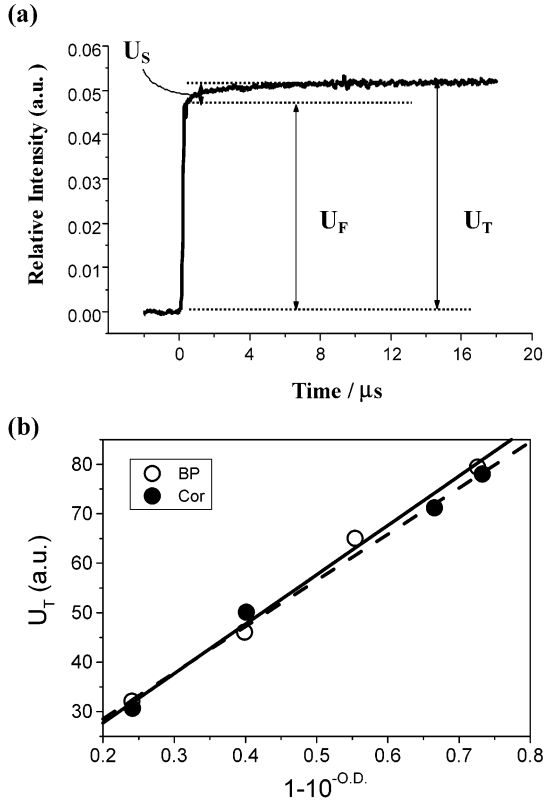

Figure 4. (a) Typical time evolution of the TR-TL signal of Cor−TEMPO (4.7 μM−0.2 mM) in benzene. U_T, U_F , and U_S are the total, fast, and slow components, respectively. (b) Plots of U_T vs $1-10^{-OD}$. Data were fitted to a linear relation, (○) BP and (●) Cor.

energy absorbed, $1-10^{-OD}$, where OD denotes the optical density at 308 nm, together with the same plots for BP. The γ value was determined as 0.94 ± 0.05. This implies that the photoreaction to form stable products and the luminescence from Cor are minor processes. Therefore, the fast-rising part is attributed to the heat from the fast radiationless transitions of Cor, namely, vibrational relaxation, IC, ISC, EIC, and EISC caused by TEMPO. The slow-rising part is due to unimolecular deactivation of ^{3}Cor* and quenching of ^{3}Cor* by TEMPO. The latter assignment is confirmed by the fact that the slow-rising part in Figure 4a is represented by a single-exponential decay with a rate constant of 2.0×10^5 s^{-1}, which agrees well with the estimated value of $k_T + k_q^T[\text{TEMPO}] = 2.2 \times 10^5$ s^{-1}. Similar agreements were found in other TR-TL data in the Cor−TEMPO systems with different TEMPO concentrations.

The Φ_T is calculated from the following equation using the relative intensity ratio of the two rising components

$$\Phi_T = \frac{U_S}{U_T}\frac{E_{ex}}{E_\Delta} \tag{15}$$

where E_Δ is the T_1 energy of Cor. The Φ_T values for various TEMPO concentrations were calculated from eq 15 with $E_{ex} =$ 32 470 cm^{-1} and $E_\Delta =$ 19 000 cm^{-1}.[26] The quantum yield at [TEMPO] = 0 mM (Φ_{isc}) was determined to be 0.64. To obtain the k_{EISC} value, the following equation, derived by considering the reactions 6−11, was used

$$\Phi_T = \frac{k_{isc} + k_{EISC}[\text{TEMPO}]}{k_f + k_q^S[\text{TEMPO}]} \tag{16}$$

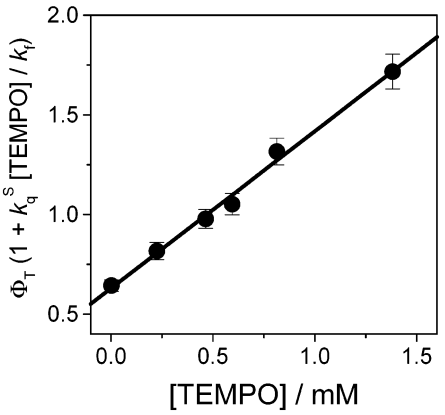

Figure 5. Plots of the value of $\Phi_T(1 + k_q^S[\text{TEMPO}]/k_f)$ against [TEMPO].

TABLE 1: Parameters for Quenching of Excited Coronene by TEMPO and S_1-T_1 ISC Quantum Yield of Coronene in Benzene

k_q^S/M^{-1} s^{-1}	k_{EISC}/ M^{-1} s^{-1}	k_q^T/M^{-1} s^{-1}	Φ_{isc}
$(4.5 \pm 0.3) \times 10^9$	$(3.2 \pm 0.4) \times 10^9$	$(0.85 \pm 0.04) \times 10^9$	0.64 ± 0.01

To minimize an error value of k_{EISC}, eq 16 was transformed to the following equation

$$\Phi_T\left(1 + \frac{k_q^S}{k_f}[\text{TEMPO}]\right) = \Phi_{isc} + \frac{k_{EISC}}{k_f}[\text{TEMPO}] \tag{17}$$

The $\Phi_T(1 + k_q^S[\text{TEMPO}]/k_f)$ values were plotted against [TEMPO] in Figure 5. The slope of the fitted line gives a value of k_{EISC}/k_f, and finally, k_{EISC} of $(3.2 \pm 0.4) \times 10^9$ M^{-1} s^{-1} was determined. All kinetic parameters determined were summarized in Table 1.

3.3. Estimation of Absolute Magnitude of Net CIDEP. The purpose of this work is to consider the mechanism of S_1 quenching by radicals on the basis of CIDEP magnitudes created by the DP-RTPM (P_n^{DP}) and the QP-RTPM (P_n^{QP}) in the Cor−TEMPO system. Therefore, we first determined P_n^{DP} value in the units of Boltzmann polarization (P_{eq}) in the presence of proper ^{3}Cor* quencher to eliminate the effect of the QP-RTPM. Then, we estimated the ratio of P_n^{QP} to P_n^{DP} ($|P_n^{QP}/P_n^{DP}|$) in the absence of the ^{3}Cor* quencher, and finally, obtained P_n^{QP} value.

Figure 6 shows CIDEP time profiles obtained in the systems of (a) BP−TEMPO and (b) Cor−TEMPO with *trans*-stilbene in benzene under the same experimental conditions. CIDEP observed in these systems are generated by the RTPM, as reported previously.[13b,14,16,17,19] In the Cor−TEMPO system, both abs and em CIDEP due to the DP- and the QP-RTPM, respectively, could appear in the time profile. In the measurement of CIDEP in the ^{1}Cor*−TEMPO system, the em CIDEP due to the QP-RTPM must be eliminated. Therefore, we used *trans*-stilbene as a triplet quencher. In this experiment, *trans*-stilbene is an appropriate molecule because (1) triplet−triplet energy transfer from ^{3}Cor* to *trans*-stilbene is exothermic and the very fast quenching rate of nearly diffusion controlled rate is expected, (2) triplet *trans*-stilbene does not create CIDEP through the QP-RTPM as previously reported,[14a] and (3) *trans*-stilbene dose not quench ^{1}Cor*. Actually, the em CIDEP signal disappears in Figure 6b as *trans*-stilbene quenches ^{3}Cor* and only the abs CIDEP due to the DP-RTPM is observed. Previously, we reported that the absolute magnitude of the net em CIDEP (P_n^{BP}) created in the BP−TEMPO system[19,21] was

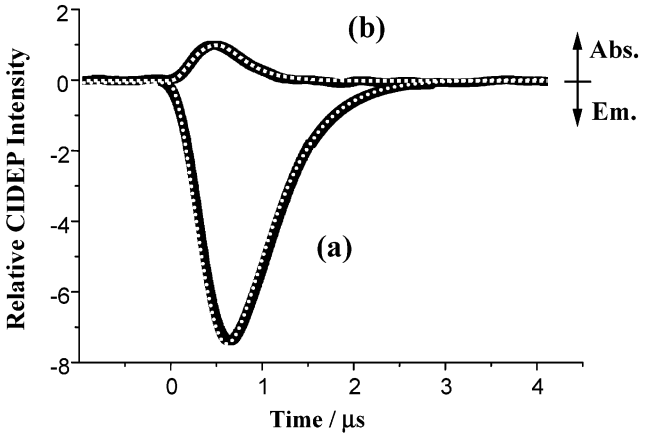

Figure 6. Time profiles of observed CIDEP signals (solid) and their simulations (dotted) of TEMPO in benzene observed at the peak of $M_I = 0$ in (a) BP (82 mM)−TEMPO and (b) Cor (0.16 mM)−TEMPO with *trans*-stilbene (1 mM) systems. Optical densities at 308 nm and TEMPO concentrations of both samples were 0.26 and 1.2 mM, respectively. Microwave power was fixed at 5 mW.

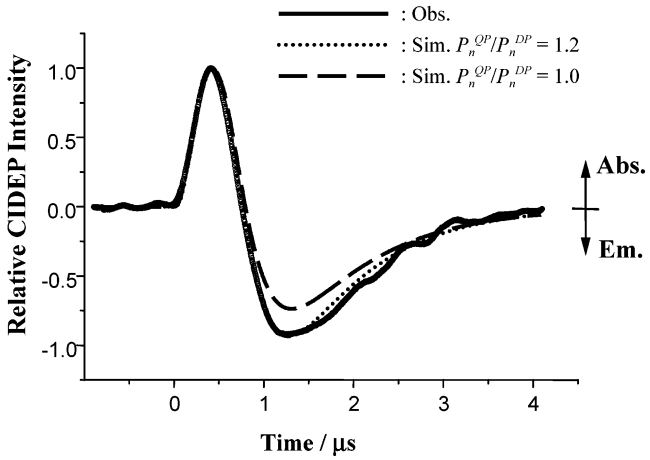

Figure 7. Observed and simulated CIDEP time profiles of TEMPO at the $M_I = 0$ peak in the Cor−TEMPO (0.16−1.2 mM) system in benzene. Microwave power was fixed at 5 mW.

$-6.9\ P_{eq}$. Thus, P_n^{DP} in the ^{1}Cor*−TEMPO interaction was determined by comparing the CIDEP signals in the ^{1}Cor*−TEMPO and BP−TEMPO systems quantitatively. Optical densities of BP and Cor at 308 nm in the 0.5-mm interior cell were adjusted at 0.26. The quantum yield of S_1-T_1 ISC of BP is 1.0.[26] Thus, the initial concentrations of excited triplet BP and ^{1}Cor* are equivalent. The TEMPO concentration was fixed at 1.2 mM, and the other experimental conditions (laser power and alignment, signal sensitivity, and microwave power) were kept constant. To determine the P_n^{DP} value, the time profiles were simulated (parts a and b of Figure 6) as follows. In the BP−TEMPO system, RTPM polarization is created on TEMPO through T_1 BP quenching by TEMPO radicals as follows

$$\mathrm{BP} + h\nu\ (308\ \mathrm{nm}) \rightarrow {}^1\mathrm{BP}^* \rightarrow {}^3\mathrm{BP}^* \quad (18)$$

$${}^3\mathrm{BP}^* \xrightarrow{k_T^{BP}} \mathrm{BP} \quad (19)$$

$${}^3\mathrm{BP}^* + \mathrm{TEMPO} \xrightarrow{k_q^{BP}} \mathrm{BP} + {}^{***}\mathrm{TEMPO} \quad (20)$$

where ^{1}BP* and ^{3}BP* represent S_1 and T_1 states of BP, respectively. The k_T^{BP} and k_q^{BP} are the rate constants of unimolecular deactivation and quenching of ^{3}BP* by TEMPO in benzene, respectively. ***TEMPO represents a radical which experienced the ^{3}BP* quenching and possesses a certain amount of CIDEP. In the above scheme, T_1-T_1 annihilation is neglected because the initial concentration ($<5 \times 10^{-5}$ M) of excited molecules is very low. An analysis is carried out by fitting the time profiles in parts a and b of Figure 6 with Bloch equations, modified with additional terms to allow for chemical kinetics and spin polarization factor (P_n) in each system. In the BP−TEMPO system, those are

$$\frac{dM_y}{dt} = -\frac{M_y}{T_2^r} + \omega_1 M_z \quad (21)$$

$$\frac{dM_z}{dt} = -\omega_1 M_y - \frac{(M_z - P_{eq}[\mathrm{TEMPO}])}{T_1^r} + P_n^{BP} k_q^{BP}[\mathrm{TEMPO}][{}^3\mathrm{BP}^*] \quad (22)$$

$$\frac{d[{}^3\mathrm{BP}^*]}{dt} = -k_q^{BP}[\mathrm{TEMPO}][{}^3\mathrm{BP}^*] - k_T^{BP}[{}^3\mathrm{BP}^*] \quad (23)$$

In the Cor−TEMPO with *trans*-stilbene system, eqs 22 and 23 are replaced by

$$\frac{dM_z}{dt} = -\omega_1 M_y - \frac{(M_z - P_{eq}[\mathrm{TEMPO}])}{T_1^r} + P_n^{DP} k_{EISC}[\mathrm{TEMPO}][{}^1\mathrm{Cor}^*] \quad (24)$$

$$\frac{d[{}^1\mathrm{Cor}^*]}{dt} = -k_q^S[\mathrm{TEMPO}][{}^1\mathrm{Cor}^*] - k_f[{}^1\mathrm{Cor}^*] \quad (25)$$

respectively. M_i represents a magnetization in the rotating frame and ω_1 is a microwave field amplitude. T_1^r and T_2^r are spin−lattice and spin−spin relaxation times, respectively. Boltzmann polarization of TEMPO could hardly be detected since the diode detector passing through a preamplifier eliminates a steady polarization as reported by Turro et al.[27] Thus, we regarded the M_y value created by an equilibrium magnetization, P_{eq}[TEMPO] as a baseline of CIDEP time profiles. The ω_1 value of our ESR cavity determined previously is 9.5×10^5 rad/s.[19] T_1^r of 250 ns was taken from the literature,[19] and T_2^r value at [TEMPO] = 1.2 mM was calculated to be 60 ns from the line width. Under the experimental condition, T_1^r, T_2^r, and ω_1 were constant in both excited molecule−TEMPO systems. In the BP−TEMPO system, reported values, $k_T^{BP} = 1.5 \times 10^5\ \mathrm{s}^{-1}$ and $k_q^{BP} = 2.0 \times 10^9\ \mathrm{M}^{-1}\ \mathrm{s}^{-1}$,[26] and the magnitude of spin polarization, i.e., $P_n^{BP} = -6.9 P_{eq}$ were used. In the Cor−TEMPO system, kinetic parameters determined above were used and a spin polarization factor of P_n^{DP} was the only variable parameter, which contributes to CIDEP intensity. From the fitting of time profiles shown in Figure 6, the $|P_n^{DP}/P_n^{BP}|$ value was estimated to be 0.26, and thus, P_n^{DP} amounts to $1.8 P_{eq}$.

Next, the absolute value of the ratio, $|P_n^{QP}/P_n^{DP}|$, was estimated by a simulation of the time profile in the Cor−TEMPO system in the absence of *trans*-stilbene as shown in Figure 7. Equation 24 is rewritten by adding a term accounting for ^{3}Cor* quenching by TEMPO as follows

$$\frac{dM_z}{dt} = -\omega_1 M_y - \frac{(M_z - P_{eq}[\mathrm{TEMPO}])}{T_1^r} + P_n^{DP} k_{EISC}[\mathrm{TEMPO}][{}^1\mathrm{Cor}^*] + P_n^{QP} k_q^T[\mathrm{TEMPO}][{}^3\mathrm{Cor}^*] \quad (26)$$

TABLE 2: Absolute Magnitudes of Net DP-RTPM and QP-RTPM Polarizations and Ratio of Magnitudes of Net Polarization in TEMPO Observed and Calculated in the Excited Coronene−TEMPO System in Benzene at Room Temperature (in Units of Boltzmann Polarization)

P_n^{QP} (obs)	P_n^{DP} (obs)	P_n^{QP} (calcd)[a]	$\lvert P_n^{QP}/P_n^{DP}\rvert$ (obs)
-2.2 ± 0.1	1.8 ± 0.1	-2.4	1.2 ± 0.1

[a] Calculated with $|3J_0| = 1 \times 10^{10}$ rad/s, $\omega_0 = 6.0 \times 10^{10}$ rad /s, $d = 7$ Å, $\alpha = 2.5$ Å^{-1}, $D_r = 5.0 \times 10^{-5}$ cm/s^2, and $\tau_c = 10$ ps. See text for details.

Equation 25 is rewritten by the following ^{3}Cor* decay kinetics

$$\frac{d[^3\text{Cor}^*]}{dt} = (\Phi_{isc} k_f + k_{EISC}[\text{TEMPO}])[^1\text{Cor}^*] - (k_T + k_q^T[\text{TEMPO}])[^3\text{Cor}^*] \quad (27)$$

where P_n^{QP} is a magnitude of net QP-RTPM spin polarization, i.e., a magnetization created through ^{3}Cor* quenching by TEMPO. The time profile in Figure 7 was simulated by numerically solving eqs 21, 25, 26, and 27 with P_n^{QP} as the only parameter, and $|P_n^{QP}/P_n^{DP}| = 1.2$ was obtained. As a comparison, a fitting curve at $|P_n^{QP}/P_n^{DP}| = 1.0$ is also shown in Figure 7, which obviously fails to reproduce the observed time profile. Similar analyses were performed for other data sets, and finally, a $|P_n^{QP}/P_n^{DP}|$ value of 1.2 ± 0.05 was determined. P_n^{QP} value was then determined to be $P_n^{QP} = -1.2P_n^{DP} = -2.2P_{eq}$ from this result. The absolute magnitudes of net DP-RTPM and QP-RTPM polarizations and the ratio in the Cor−TEMPO system were summarized in Table 2.

3.4. Theoretical Calculation of Spin Polarization. CIDEP is deeply related to intermolecular potential and spin dynamics of a radical−excited molecule encounter complex. The experimental values P_n^{DP}, P_n^{QP}, and $|P_n^{QP}/P_n^{DP}|$ are therefore useful in describing the quenching dynamics. Here, we discuss the spin polarizations on the basis of the analytical formula proposed for net CIDEP generation by the RTPM.[17,22] According to the relaxational mechanism proposed by Shushin,[22a] a nonadiabatic Q−D transition induced by a fluctuating zfs interaction is considered in RT pair with their exponentially decaying exchange interaction given by a formula

$$J(r) = J_0 \exp\{-\alpha(r - d)\} \quad (28)$$

where d is a distance of the closest approach in the RT pair. Shushin derived simple analytical formulas for the two limiting cases of the J_0 value, (1) a strong exchange interaction case, $|3J_0| \gg \omega_0$, and (2) a weak exchange interaction case, $|3J_0| \ll \omega_0$, where the ω_0 is Zeeman energy. First, we calculated P_n^{QP} values and compared them to the experimental value to find whether exchange interaction of the ^{3}Cor*−TEMPO pair belongs to case 1 or 2. Analytical formulas for strong and weak exchange interactions are, respectively, given by

$${}^sP_n^{QP} = -\frac{\pi}{45}\frac{D_{zfs}^2}{\omega_0^2}\frac{\omega_0 d}{\alpha D_r}\left(\frac{1}{1+x^2} + \frac{4}{4+x^2}\right)\frac{d}{r_{QP}} \quad (29)$$

and

$${}^wP_n^{QP} = -\frac{8}{45}\frac{D_{zfs}^2}{\omega_0^2}\frac{(3J_0)dx}{\alpha D_r}\left(\frac{1}{(1+x^2)^2} + \frac{4}{(4+x^2)^2}\right)\frac{d}{r_{QP}} \quad (30)$$

where $x = 1/\omega_0\tau_c$. In calculations of eqs 29 and 30 to evaluate P_n^{QP} values, $\omega_0 = g\beta B_0 = 6.0 \times 10^{10}$ rad/s and the reported D_{zfs} value[26] of 1.8×10^{10} rad/s for ^{3}Cor* were used. The diffusion coefficient of Cor in benzene was assumed to be 2.5×10^{-5} cm/s^2 because the molecular radius of Cor is almost the same as that of BP, whose diffusion constant in benzene is reported to be 2.5×10^{-5} cm/s^2 at room temperature.[28] The diffusion coefficient of TEMPO was also assumed to be 2.5×10^{-5} cm/s^2 (and thus $D_r = 5.0 \times 10^{-5}$ cm/s^2).[19] The correlation time τ_c was estimated as 10 ps from the diffusion constant of Cor. For potential parameters, $d = 7$ Å and $\alpha = 2.5$ Å^{-1} were used and J_0 values in eqs 29 and 30 were assumed to be $|^3J_0| = 1 \times 10^{12}$ ($|^3J_0| \gg \omega_0$) and $|^3J_0| = 5 \times 10^9$ rad/s ($|^3J_0| \ll \omega_0$), respectively. From eq 28, separations between the radical and triplet molecule at the level crossing were estimated as $r_1 = 7.8$ Å and $r_2 = 8.1$ Å. The r_{QP} is treated as a distance between ^{3}Cor* and TEMPO when ^{3}Cor* quenching occurs and $r_{QP} \approx d$ is assumed. From eqs 29 and 30, P_n^{QP} values were calculated as ${}^sP_n^{QP} = -2.4P_{eq}$ and ${}^wP_n^{QP} = -0.16P_{eq}$, respectively. The ${}^sP_n^{QP}$ value sufficiently agrees with the P_n^{QP} value of $-2.2P_{eq}$ determined in this work. The calculated ${}^wP_n^{QP}$ value is much smaller than the experimental value of $-2.2P_{eq}$, and it is therefore concluded that exchange interaction of the ^{3}Cor*−TEMPO pair should be much larger than Zeeman energy and the net CIDEP is dominantly created in the level-crossing regions.

The relaxational mechanism for the QP-RTPM assumes that RT pairs are created isotropically at a certain distance of r_{QP} in the Q states ($|Q_{\pm 3/2}\rangle$, $|Q_{\pm 1/2}\rangle$) and populations of the $|D_{\pm 1/2}\rangle$ states are negligible.[22a] It is noted that the net abs and em CIDEPs observed in the Cor−TEMPO system were generated on the same potential surface of the RT pair with the same CIDEP mechanism, namely, the RTPM, except for spin multiplicity of the precursor RT pairs. We applied the relaxational mechanism for the DP-RTPM, in which RT pairs were assumed to be created isotropically at a distance of r_{DP} in $|D_{\pm 1/2}\rangle$ states. P_n^{DP} values derived by applying the strong exchange interaction case is given by

$$P_n^{DP} = \frac{\pi}{45}\frac{D_{zfs}^2}{\omega_0^2}\frac{\omega_0 d}{\alpha D_r}\left(\frac{1}{1+x^2} + \frac{4}{4+x^2}\right)\frac{d}{r_{DP}} \quad (31)$$

The parameters in eqs 29 and 31 are the same except for r_{QP} and r_{DP}. In this case, $|P_n^{QP}/P_n^{DP}|$ is represented by an inverse ratio of the distances as follows

$$\left|\frac{P_n^{QP}}{P_n^{DP}}\right| = \frac{r_{DP}}{r_{QP}} \quad (32)$$

Therefore, the $|P_n^{QP}/P_n^{DP}|$ value obtained in the present study gives $r_{DP} = 1.2r_{QP}$. If r_{QP} is nearly equivalent to the distance of the closest approach assumed here, i.e., $r_{QP} \approx 7$ Å, r_{DP} is calculated to be 8.4 Å, which locates outside of the level-crossing point, r_2. This result implies that the reaction distance of S_1-T_1 EISC in the ^{1}Cor*−TEMPO pair is about 1.4 Å longer than that of ^{3}Cor* quenching. Exchange interaction should decrease as a distance becomes longer, and thus, exchange interaction of the ^{3}Cor*−TEMPO pair at r_{DP} is smaller than that at r_{QP}. ^{3}Cor* quenching occurs solely by exchange interaction of collision complex as reported previously[2,3] and k_q^T is smaller than k_{EISC}. This means that the S_1-T_1 EISC mechanism is slightly different from the ^{3}Cor* quenching. We discuss this interesting point in the following.

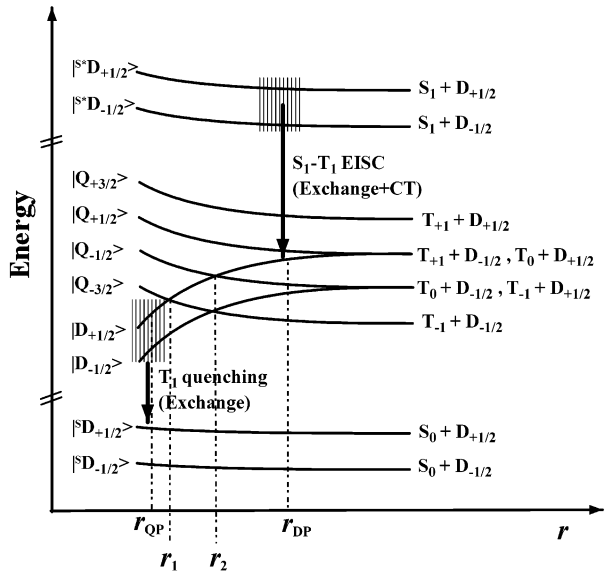

Figure 8. Schematic diagram of excited Cor quenching by TEMPO.

3.5. Enhanced S_1-T_1 ISC Mechanism. To understand the reason the rate constant for S_1-T_1 EISC is larger than that for T_1 quenching in the Cor−TEMPO system, we examine the effect of CT interaction in ^{1}Cor* quenching by TEMPO in benzene. CT state energy, E_{CT}, at the solvent coordinate where the S_1−TEMPO pair is at minimum energy is given by the following equation[29]

$$E_{CT} = \{ E^{ox}_{1/2}(\text{TEMPO}) - E^{red}_{1/2}(\text{Cor}) + \Delta E_{corr} \} + \{\lambda(r) - E_{coulomb}(r)\} \quad (33)$$

where $E^{ox}_{1/2}$(TEMPO) and $E^{red}_{1/2}$(Cor) mean half-wave redox potentials of TEMPO (+0.64 V)[30] and Cor (−2.07 V)[26] vs the standard calomel electrode in CH_3CN. In CT quenching, TEMPO is considered as an electron donor due to its low oxidation potentials. Since these redox potentials were obtained in polar solvent ($\epsilon = 35.94$), we added a correction term, ΔE_{corr} of 0.64 eV in benzene ($\epsilon = 2.284$), estimated by the Born equation for solvation energies of ions with their radius of 3.5 Å.[29a] The $\lambda(r)$ is a solvent reorganization energy between the S_1−TEMPO pair and the CT complex, and $E_{coulomb}(r)$ is the Coulomb energy of the CT state. Both values depend on the Cor−TEMPO distance, r. The $\lambda(r)$ value of 0.012 eV was calculated by assuming Marcus's formula of $\lambda(r)$[31] with $r_A = r_D = 3.5$ Å, $r_{AD} = 7$ Å, $n = 1.50$, and $\epsilon = 2.284$. The $E_{coulomb}(r)$ is 0.90 eV with $r_{AD} = 7$ Å in benzene. According to these values, we obtained an E_{CT} value of 2.46 eV. This value is smaller and larger than energies of ^{1}Cor* (2.91 eV) and ^{3}Cor* (2.36 eV), respectively. Thus, S_1-T_1 EISC with CT interaction is exothermic, while ^{3}Cor* quenching through the CT interaction is endothermic. According to the general approach of Rehm−Weller for CT quenching,[32] the rate constant for an exothermic process may be 10^9-10^{10} M^{-1} s^{-1}, which is the same order with the k_{EISC} value in the present work. On the other hand, the rate constant for an endothermic process is slower than the diffusion-controlled rate, suggesting that ^{3}Cor* quenching occurs solely by exchange interaction.

The quenching processes for both S_1 and T_1 states are schematically summarized in Figure 8. In T_1 quenching, RT pairs of $|D_{\pm1/2}\rangle$ states undergo deactivation to be $|^SD_{\pm1/2}\rangle$ states at the distance, r_{QP}, while RT pairs of $|Q_{\pm3/2}\rangle$ and $|Q_{\pm1/2}\rangle$ states remain unchanged. Therefore, RT pairs of $|Q_{\pm3/2}\rangle$ and $|Q_{\pm1/2}\rangle$ states may exist predominantly in the region inside the level crossings ($r < r_1$). On the other hand, RT pairs generated through S_1-T_1 EISC may exist predominantly in the regions outside the level crossings ($r > r_2$) as discussed above. Considering eq 31, in which a magnitude of polarization is in inverse proportion to an initial distance of the RT pair (r_{DP}), the magnitude of net polarization generated in S_1-T_1 EISC must be smaller than that in T_1 quenching. Exchange mechanism for quenching contributes to both S_1-T_1 EISC and T_1 quenching while CT quenching may contribute additionally to S_1-T_1 EISC, which results in a larger rate constant of S_1-T_1 EISC than that of T_1 quenching. This indicates that the mean reaction distance in S_1-T_1 EISC is larger than that of T_1 quenching. This is along with the quenching model predicted by CIDEP analysis, namely, r_{DP} is larger than r_{QP} and T_1 quenching occurs through strong exchange interaction.

The present study on CIDEP demonstrates that the $|P^{QP}_n/P^{DP}_n|$ value could be useful in the studies of S_1-T_1 EISC processes by free radicals. Since it is not always possible to distinguish CT and exchange mechanisms by examining the rate constants, additional information given by CIDEP analysis will be useful in the study of quenching processes. An expanded CIDEP study on S_1-T_1 EISC processes for molecular systems with various energy gaps between S_1 and CT states are now in progress by judging both rate constants and $|P^{QP}_n/P^{DP}_n|$ values.

Acknowledgment. This work was supported in part by a Grant-in-Aid for Scientific Research (No. 15550005) from the Ministry of Education, Science, Culture and Sports of Japan.

References and Notes

(1) Gijzemann, O. L. J.; Kaufmann, F.; Porter, G. *J. Chem. Soc., Faraday Trans. 2* **1973**, *69*, 727.
(2) (a) Kuzumin, V. A.; Tatikolov, A. S. *Chem. Phys. Lett.* **1977**, *51*, 45. (b) Kuzumin, V. A.; Tatikolov, A. S. *Chem. Phys. Lett.* **1978**, *53*, 606.
(3) Watkins, A. R. *Chem. Phys. Lett.* **1980**, *70*, 262.
(4) Tatikolov, A. S.; Levin, P. P.; Kokrashvilli, T. A.; Kuzumin, V. A. *Bull. Acad. Sci. USSR* **1983**, *3*, 465.
(5) Watkins, A. R. *Chem. Phys. Lett.* **1974**, *29*, 526.
(6) Karpiuk, J.; Grabowski, Z. *Chem. Phys. Lett.* **1989**, *160*, 451.
(7) Weiss, D. S. *J. Photochem.* **1976/1977**, *6*, 301.
(8) (a) Green, J. A., II; Singer, L. A.; Parks, J. H. *J. Chem. Phys.* **1973**, *58*, 2690. (b) Green, J. A., II; Singer, L. A. *J. Am. Chem. Soc.* **1974**, *96*, 2730.
(9) Chattopadhyay, S. K.; Das, P. K.; Hug, G. L. *J. Am. Chem. Soc.* **1983**, *105*, 6205.
(10) Suzuki, T.; Obi, K. *Chem. Phys. Lett.* **1995**, *246*, 130.
(11) (a) Corvaja C.; Maggini M.; Prato M.; Scorrano G.; Venzin M. *J. Am. Chem. Soc.* **1995**, *117*, 8857. (b) Ishii, K.; Fujisawa, J.; Ohba, Y.; Yamauchi, S. *J. Am. Chem. Soc.* **1996**, *118*, 13079. (c) Teki, Y.; Miyamoto, S.; Nakatsuji, M.; Miura, Y. *J. Am. Chem. Soc.* **2001**, *123*, 294. (d) Asano-Someda, M.; van der Est, A.; Krgüer, U., Stehlik, D.; Kaizu, Y.; Levanon, H. *J. Phys. Chem. A* **1999**, *103*, 6704.
(12) Ballesteros, O. G.; Maretti, L.; Sastre, R.; Scaiano, J. C. *Macromolecules* **2001**, *34*, 6184.
(13) (a) Blättler, C.; Jent, F.; Paul, H. *Chem. Phys. Lett.* **1990**, *166*, 375. (b) Kawai, A.; Okutsu, T.; Obi, K. *J. Phys. Chem.* **1991**, *95*, 9130.
(14) (a) Kawai, A.; Obi, K. *J. Phys. Chem.* **1992**, *96*, 52. (b) Kobori, Y.; Kawai, A.; Obi, K. *J. Phys. Chem.* **1994**, *98*, 6425.
(15) Kawai, A.; Obi, K. *J. Phys. Chem.* **1992**, *96*, 5701.
(16) Kawai, A.; Obi, K. *Res. Chem. Intermed.* **1993**, *19*, 865.
(17) Goudsmit, G. H.; Paul, H.; Shushin, A. I. *J. Phys. Chem.* **1993**, *97*, 19243.
(18) Goudsmit, G. H.; Paul, H. *Chem. Phys. Lett.* **1993**, *73*, 208.
(19) Kobori, Y.; Mitsui, M.; Kawai, A.; Obi, K. *Chem. Phys. Lett.* **1996**, *252*, 355.
(20) (a) Mitsui, M.; Takeda, K.; Kobori, Y.; Kawai, A.; Obi, K. *Chem. Phys. Lett.* **1996**, *262*, 125. (b) Fujisawa, J.; Ohba, Y.; Yamauchi, S. *J. Phys. Chem. A* **1997**, *101*, 434. (c) Kawai, A. *Appl. Magn. Reson.* **2003**, *23*, 349.
(21) Kobori, Y.; Takeda, K.; Tsuji, K.; Kawai, A.; Obi, K. *J. Phys. Chem. A* **1998**, *102*, 5160.
(22) (a) Shushin, A. I. *Chem. Phys. Lett.* **1993**, *208*, 173. (b) Shushin, A. I. *J. Chem. Phys.* **1992**, *97*, 3171. (c) Shushin, A. I. *J. Chem. Phys.* **1993**, *99*, 8723.

(23) Adrian, F. J. *Chem. Phys. Lett.* **1994**, *229*, 465.
(24) Suzuki, T.; Kajii, Y.; Shibuya, K.; Obi, K. *Res. Chem. Intermed.* **1991**, *15*, 261.
(25) Kajii, Y.; Fujita, M.; Hiratuska, H.; Obi, K.; Mori, Y.; Tanaka, I. *J. Phys. Chem.* **1987**, *91*, 2791.
(26) Murov, S. L.; Carmichael, I.; Hug, G. L. *Handbook of photochemistry*; Marcel Dekker, Inc.: New York, 1993.
(27) Turro, N. J.; Koptyug, I. V.; Willingen, H. V.; McLauchlan, K. A. *J. Magn. Reson.* **1994**, *109*, 121.
(28) Terazima, M.; Okamoto, K.; Hirota, N. *J. Phys. Chem.* **1991**, *95*, 9080.
(29) (a) Kawai, A.; Shibuya, K. *J. Phys. Chem. A* **2002**, *106*, 12305. (b) Kawai, A.; Watanabe, Y.; Shibuya, K. *Chem. Phys. Lett.* **2003**, *372*, 8.
(30) Samanta, A.; Bhattacharyya, K.; Das, P. K.; Kamat, P. V.; Weir, D.; Hug, G. L. *J. Phys. Chem.* **1989**, *93*, 3651.
(31) (a) Marcus, R. A. *J. Chem. Phys.* **1956**, *24*, 966. (b) Marcus, R. A. *J. Chem. Phys.* **1957**, *26*, 867.
(32) Rehm, D.; Weller, A. *Isr. J. Chem.* **1970**, *8*, 259.